ACS NANO

www.acsnano.org

ARTICLE

Nanopillar Arrayed Triboelectric Nanogenerator as a Self-Powered Sensitive Sensor for a Sleep Monitoring System

Weixing Song,[†] Baoheng Gan,[†,‡] Tao Jiang,[†] Yue Zhang,[†] Aifang Yu,[†] Hongtao Yuan,[†] Ning Chen,[‡] Chunwen Sun,[*,†] and Zhong Lin Wang[*,†,§]

[†]Beijing Institute of Nanoenergy and Nanosystems, Chinese Academy of Sciences, National Center for Nanoscience and Technology (NCNST), Beijing 100083, China

[‡]School of Materials Science and Engineering, University of Science and Technology Beijing, Beijing 100083, China

[§]School of Materials Science and Engineering, Georgia Institute of Technology, Atlanta, Georgia 30332, United States

Supporting Information

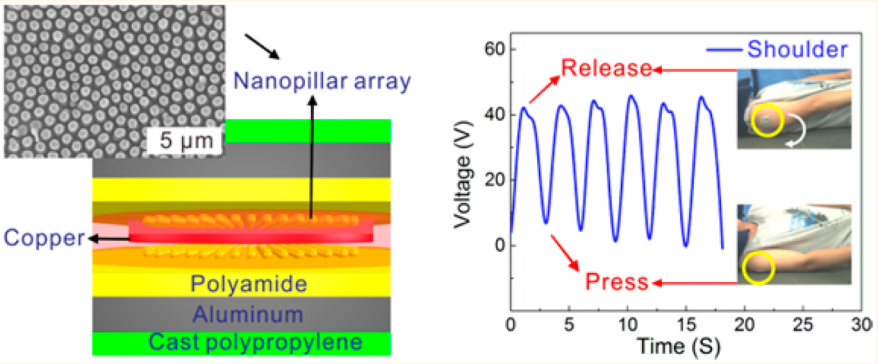

ABSTRACT: **A flexible and low-cost triboelectric nanogenerator (TENG) based on a patterned aluminum−plastic film and an entrapped cantilever spring leaf is developed as a self-powered sensitive triboelectric sensor for sleep−body movement monitoring. The working mechanism and the impact factors of electric output performance were systematically investigated and elaborated. Due to the patterned nanostructures of the recently designed TENG, both the output voltage and current are greatly enhanced, and thereby the sensitivity of the device is significantly improved. The self-powered and sensitive device has been demonstrated as a smart body motion sensor of sleep monitoring for diagnosis of sleep disorders due to its high sensitivity and excellent stability. This work may promote the application of self-powered TENGs for healthcare and be helpful for the development of real-time mobile healthcare services and smart external portable electronics.**

KEYWORDS: *triboelectric nanogenerator, self-powered sensor, nanopillar array, thermoplastic forming method, anodic aluminum oxide template*

Sleep disorder is a major health problem affecting many people, and its common clinical diagnosis is based on the use of sensors for airflow breathing, breathing movements of the thorax, body movements, and so on.[1−3] The monitoring devices generally require bulky battery packs or continuous use of electricity by an electric plug in order to achieve extreme sensitivities. In addition, exactly detecting body movements caused by sleep apnea, especially for kids who spend a large amount of time sleeping, is extremely difficult with these devices. Thus, a smart sensor that can drive itself without an additional supply source is highly desirable. Herein, we introduce an effective approach to solving the problem by using a sensitive and self-powered triboelectric nanogenerator (TENG), inspired by the rapid development of TENGs as sensitive sensor devices.[4−8] TENGs have been widely applied in converting mechanical energy into electricity.[9−16] Moreover, they can also serve as self-powered sensors due to the high sensitivity of contact between two materials with different triboelectric polarities.[6,17−21] For example, a TENG was smartly designed as a self-powered communication unit for processing and transmitting information.[18] A fully packaged TENG based on hemisphere arrays can be utilized as a self-powered

Received: June 30, 2016
Accepted: August 5, 2016

DOI: 10.1021/acsnano.6b04344
ACS Nano XXXX, XXX, XXX−XXX

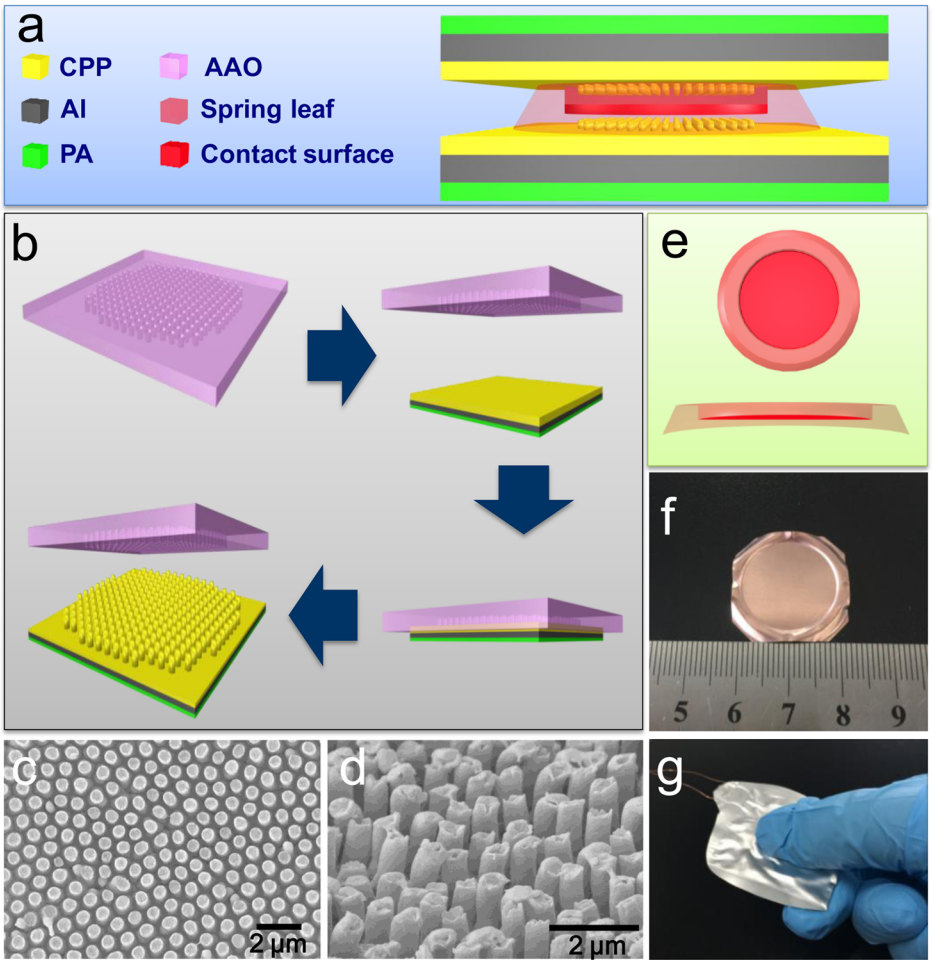

Figure 1. (a) Schematic of the TES. (b) Fabrication process of the nanopillar arrays on an APLF surface. SEM images of (c) top view and (d) side view of nanopillar arrays. (e) Schematic of the cantilever spring leaf (top) and cross section profile (bottom). (f) Optical photo of a typical cantilever spring copper leaf. (g) Optical photo of a TES. The spring leaf is schematized transparent for clear illustration in (a) and (e).

triboelectric pressure sensor to map the distribution of foot produced pressure.[20] These devices are designed with the same working mechanism based on triboelectric effect and electrostatic induction. The mechanical contact and separation between two separate components can induce charge and produce an electric potential difference which drives an electron current in the external circuit. Various materials with different triboelectric polarities have already been utilized to produce an electric output and improve the efficiency of the devices. Generally, a thin polymer film such as polyimide (Kapton),[22,23] polytetrafluoroethylene (PTFE),[11,24] polydimethylsiloxane (PDMS),[25,26] and fluorinated ethylene propylene (FEP)[27,28] is chosen to serve as a triboelectric layer of a TENG. It should be noted that a surface of the polymer film has to be in tight contact with the metal layer in order to induce and transfer charge. In practice, sputtering is usually applied to deposit metal on the surface of the polymer film,[29−31] but the deposited films with high cost tend to suffer from abrasion and scratching.

Herein, we introduce a sensitive TENG based on an aluminum−plastic laminated film (APLF) serving as a self-powered device for body-movement sensing and sleep monitoring. The sensors can generate a much stronger output than the sensors based on a piezoelectric nanogenerator for tracking eye ball motion.[32] An APLF is generally used as a packaging material for flexible pouch batteries. Herein, an APLF-fabricated TENG can produce strong electric signals and thus be used as a self-powered triboelectric sensor (TES). The TENG has a sandwich structure that consists of a folded APLF and a 2 mm cantilever spring leaf inside the folded APLF and creates two equal friction pairs on both sides of the leaf, as shown in Figure 1a. An intermediate aluminum layer inside the APLF and the cantilever spring leaf serve as two electrodes of the TENG. By introducing a nanopillar array structure on the contact surface of the APLF, the sensitivity of the TES is obviously strengthened. The spring leaf made of a whole flexible 50 μm copper piece has a middle concave plane supported by four legs with a height of 1 mm (Figure 1e). During pressing, the top part of the APLF contacts and presses the middle plane, thereby contacting the bottom part of the APLF. Due to elasticity of the metal, the pressed middle plane would immediately rebound and automatically recover once the pressure is released. With these features of the structure, the TES can sensitively respond in real time to the pressure change caused by body movements of humans during sleep. Meanwhile, the TENG can trigger light-emitting diodes (LEDs) for security notification without using external power sources. Therefore, this work presents potential applications of the TENGs in healthcare and movement monitoring as well as safety monitoring.

DOI: 10.1021/acsnano.6b04344
ACS Nano XXXX, XXX, XXX−XXX

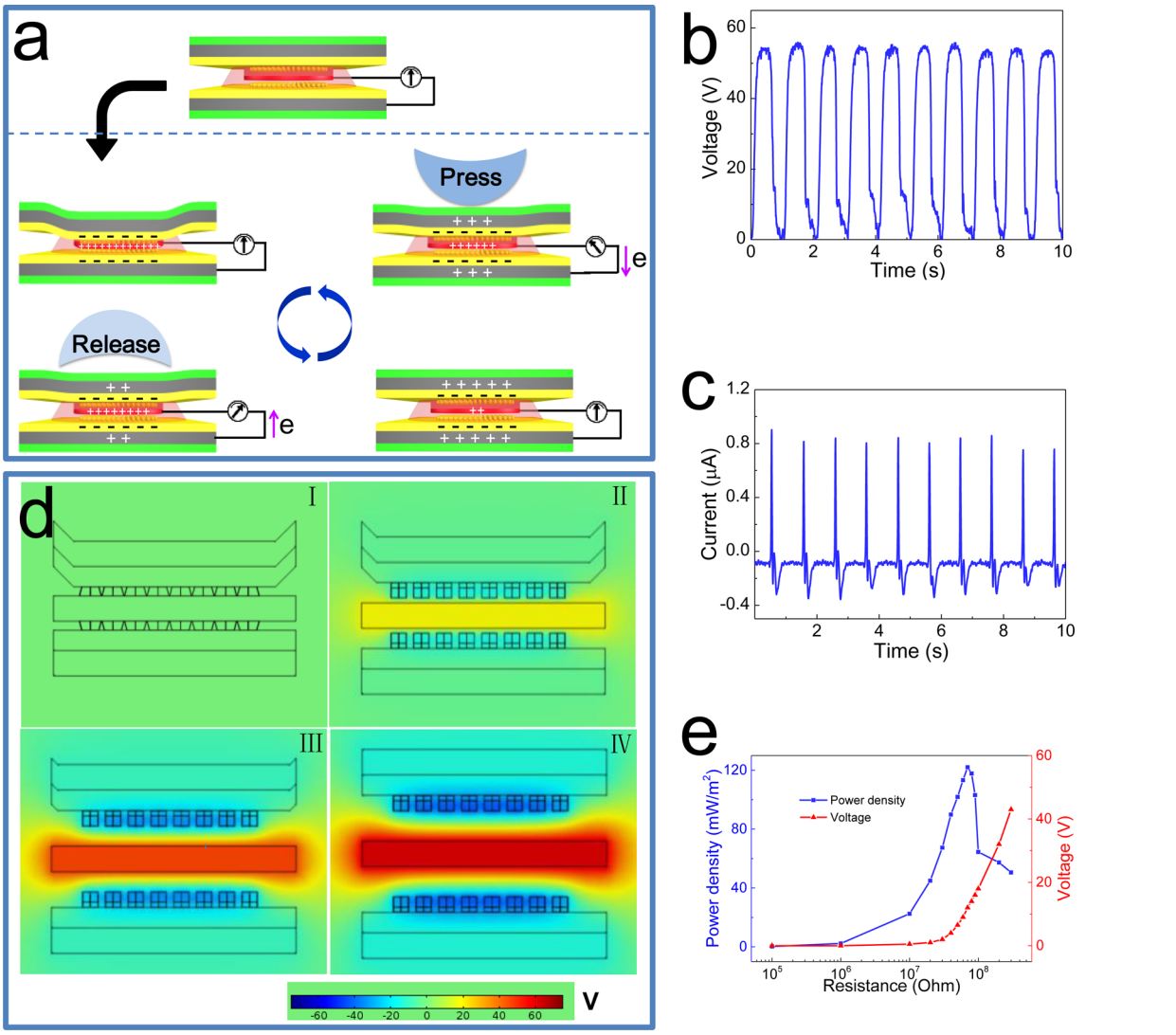

Figure 2. (a) Schematic illustration of the working mechanism of the TENG based on APLF. (b) Output open-circuit voltage (V_{oc}) and (c) short-circuit current of the TENGs. (d) Electric potential distributions for typical separation distances between the two electrodes. (e) Output power density and V_{oc} with different external load resistances.

RESULTS AND DISCUSSION

The APLF with a thickness of about 100 μm is mainly composed of a polyamide layer, an aluminum layer, and a cast polypropylene (CPP) layer. The TENG with APLF nanopillar array structures is schematically illustrated in Figure 1a. A cantilever spring leaf copper is clamped by two pieces of APLF. To improve sensitivity of the TENGs, vertically aligned CPP nanopillar arrays were formed on the APLF surface. The fabrication process of the nanopillar arrays is schematically described in Figure 1b. The CPP nanopillar arrays were obtained *via* a thermoplastic forming method by using anodic aluminum oxide (AAO) templates (Figure S1). SEM images show that the CPP nanopillar arrays are evenly distributed on the surface of the APLF after being pressed for 10 min at 18 °C (Figure 1c,d). They have a uniform diameter of about 600 nm and a length of 1.5 μm along the 700 nm diameter pore of the AAO template. The nanopillars with diameters of 350 nm were obtained using the AAO template with a pore diameter of about 400 nm (Figure S2b). The pillar diameter is slightly smaller than the pore diameter of the AAO template because the pillars shrink at room temperature, thereby enabling easy peeling of the CPP from the AAO template. In this TENG design, the homemade cantilever spring leaf plays an important role. It not only serves as an electrode of the TENG but also supports the APLF to stay away from the middle concave plane of the leaf. In response to pressing, both inside surfaces of the APLF with nanopillar arrays contact the two surfaces of the middle copper plane, and thus two friction pairs work. Once the pressing is released, both the middle concave plate and the APLF will automatically recover and separate. Figure 1g shows an optical photo of the whole fabricated TENG, where the middle concave plane has a circular contact area of about 1.8 cm^2 (Figure 1f).

The working mechanism of the TENG is schematically described in Figure 2. The device works by relying on the coupling between the triboelectric effect and electrostatic induction.[4,5,21,33−35] Considering the difference of triboelectric polarities between CPP and copper, electrons will transfer from the copper surface to the CPP layer during contacting caused by pressing. The top CPP layer contacts the middle copper plane, and the middle plane deforms and dents, leading to further direct contact with the bottom CPP layer. Surface

DOI: 10.1021/acsnano.6b04344
ACS Nano XXXX, XXX, XXX−XXX

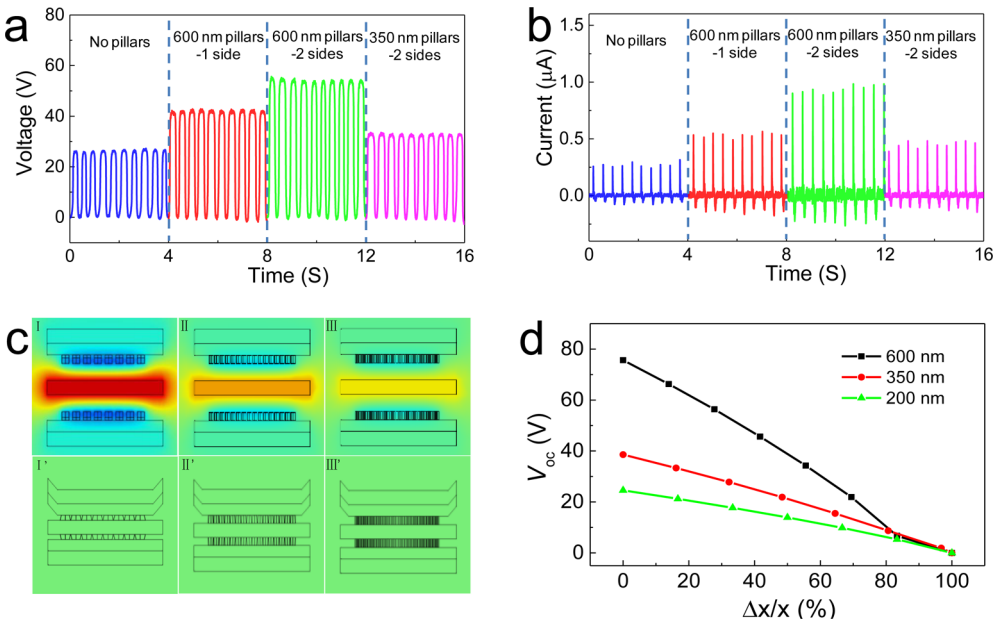

Figure 3. Comparison of the (a) open-circuit voltage and (b) short-circuit current of TENGs with different nanopillar arrays. (c) Electric potential distribution at the largest separation (I, II, III) and the contact states (I′, II′, III′) on surfaces of two electrodes with different nanopillar diameters of 600 nm (I, I′), 350 nm (II, II′), and 200 nm (III, III′), respectively. (d) Plots of V_{oc} of TENGs with various diameters of nanopillars as a function of deformation ratio ($\Delta x/x$).

charge transfer then takes place at the contact area due to triboelectrification.[21] As a result, the two friction pairs are electrostatically charged with opposite charges. After releasing the pressure, the friction pairs separate, caused by the rapid rebound of the middle copper plane, resulting in a potential difference between the APLF electrode and the copper electrode. During release, electrons will transfer *via* an external circuit between two electrodes driven by the generated triboelectric potential difference, representing a current flow from the copper electrode to the APLF electrode (Figure 2a). The electric potential difference across the two electrodes can be expressed by eq 1.[21,36]

$$V = \frac{\sigma d}{\varepsilon_o} \tag{1}$$

where σ is the triboelectric charge density, ε_o is the vacuum permittivity, and d is the distance between two electrodes. The variation in potential difference drives the electron flow between the two electrodes.

Figure 2b,c presents the typical trends in changes of open-circuit voltage (V_{oc}) and short-circuit current (I_{sc}). The V_{oc} increases when the potential difference increases, caused by enlarging the separation (Figure 2b). The average V_{oc} and I_{sc} produced by the 1.5 μm CPP nanopillar-based TENG are about 55 V and 0.9 μA, respectively. To clarify the effect of nanopillars with different sizes on the output performance of the TENGs, the electric potential distribution and the charge transfer between the two electrodes were investigated *via* finite-element simulation using COMSOL Multiphysics software. Figure 2d shows the calculated electric potential distributions at typical steps during the contact separation. The electric potential difference between the two electrodes increases as the separation increases. By loading different external resistances, the performance of the TENG was examined, as well. The power density reaches a maximum value with an external load of 60 MΩ. According to the maximum power transfer theorem,[37,38] the internal resistance of the TES is determined to be around 60 MΩ.

The structure of CPP nanopillars exerts great influence on the triboelectric effect. The nanopillars having lengths of more than 3 μm tend to bend and thereby reduce the triboelectric effect (Figure S3). For nanopillars with lengths from 1 to 3 μm, there is no obvious difference in output performance. Comparison of the output performance between TENGs with one and two surfaces of CPP nanopillars further demonstrates that the nanopillar arrays on the APLF enhance the triboelectric effect, and thus the TENG shows remarkable voltage and current output (Figure 3a,b). The unstructured CPP layers exhibit weak sensitivity in response to the pressure because the CPP layers cannot be elastically displaced.[39] Compared with the V_{oc} of 26 V for the unstructured layer, the value for the layer with a 600 nm nanopillar array on both sides has more than doubled to 55 V. On the contrary, the nanopillar arrays on the CPP layers behave like a spring and contribute to much easier charge separation. Moreover, the structured CPP layers with the significantly increased surface area and more complicated surfaces can generate more surface charges during friction and thus exhibit a larger effective triboelectric effect. Therefore, the increased σ caused by the nanopillar arrays on CPP layers results in higher open-circuit voltage according to eq 1. The generated current I can be determined by eq 2.[40]

$$I = \frac{dQ}{dt} = C\frac{\partial V}{\partial t} + V\frac{\partial C}{\partial t} \tag{2}$$

where Q is the charge of the system, C is the capacitance of the device, and V is the voltage across the two electrodes. The two parts refer to the variation in the electric potential difference caused by the triboelectric charges and the variation in capacitance caused by the change of distance between the two electrodes. The devices with the nanopillar arrays generate a higher short-circuit current, as shown in Figure 3b. The current for the structured CPP layer with a 600 nm nanopillar

DOI: 10.1021/acsnano.6b04344
ACS Nano XXXX, XXX, XXX−XXX

array on both sides is about triple that of the unstructured layer. It is obviously caused by the improved capacitance of the devices with the structured layers due to the increased surface area. Another important factor is the improved change in capacitance between two friction layers during compression and release. The phenomenon can be attributed to the fact that the changed volume is air with lower permittivity during pressing and releasing.[39] As a result, the CPP layers with the 600 nm nanopillar arrays induce the TENGs to produce a current output 3 times higher than that of the TENGs with unpatterned layers.

Another important parameter of the dimension for the triboelectrification effect is the pillar diameter. For comparison, the V_{oc} and I_{sc} of TENGs based on nanopillars with diameters of 350 and 600 nm are also shown in Figure 3a,b. The voltage and current output of TENGs significantly increase as the diameter of nanopillars becomes larger. The results can mainly be attributed to the following two factors. The average gap between the 350 nm nanopillars is about a quarter of the pillars diameter, and the value is half of that for 600 nm nanopillars (Figures S1 and S2). When being pressed, the 600 nm nanopillars easily deform and the side of the top part of the pillars can also contact another electrode. Therefore, the contact surface area is obviously increased. The 350 nm nanopillars cannot be significantly pressed and provide more elastic resistance, thus producing less triboelectric charges on the contact surface. Moreover, the better elasticity caused by the larger pillars and wider gaps leads to easier charge separation.[40] In addition, the nanopillar arrays with smaller diameters tend to bend and easily affect the stability of the device. We further verified and compared the electric potential distributions between the TENGs based on different nanopillar arrays with 600, 350, and 200 nm diameters at separation and contact states, as illustrated in Figure 3c. Figure 3d presents the calculated V_{oc} for the TENGs based on different nanopillar arrays with 600, 350, and 200 nm diameters as a function of the deformation ratio ($\Delta x/x$). The electric potential difference between the two electrodes decreases as the deformation depth (Δx) increases. It can also be seen that the V_{oc} increases with the increase in diameters of nanopillars because the triboelectric charge density σ increases by increasing the total amount of transferred charges due to the enlarged contact surface area.

The flexibility and special property of the APLF provide more potential applications for TENGs. The flat and thin TENG can be easily fixed on any surface. Moreover, it can be deformed easily and recovered after release due to its flexibility (Figure 4a-I). Besides serving as an electrode of the TENG, the APLF can also be conveniently packaged in order to prevent the inside metal electrode from oxidation and corrosion. The copper electrode inserted into the folded APLF is free from air and water, so the durability is improved after packaging (Figure 4a-II,b).[41] The TENGs were periodically pressed under different operating frequencies from 0.5 to 2 Hz, and the output voltage remained constant. Furthermore, the constant output voltage and current signals were obtained after numerous repeated operations (Figure 4c), which points out that a high stability of the devices is achieved, as well. As a result, the sandwich structures not only enhance the TES performance but also make it convenient for packaging. The energy produced by the TES can drive many LED lights simultaneously, as shown in Figure 4a. In addition, the sealed TENG is also waterproof due to hot-sealing of APLF (Figure S4). Therefore, due to these remarkable advantages of the

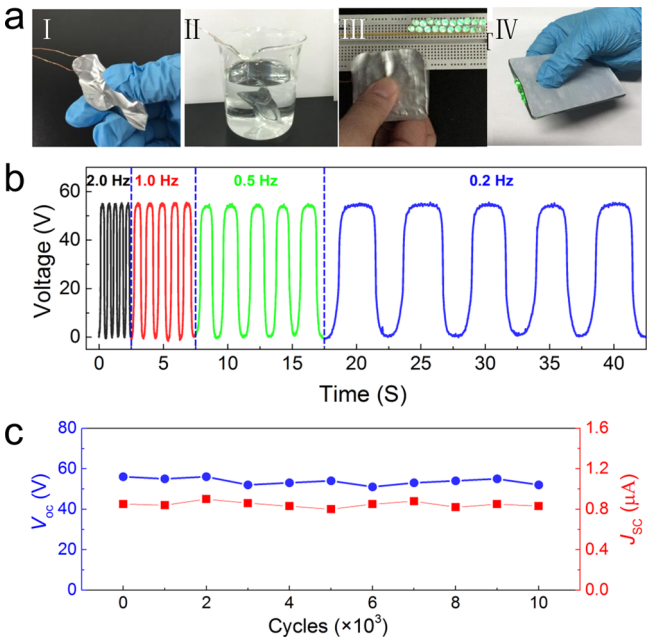

Figure 4. (a) Photograph of (I) the bent TENG, (II) the TENG soaked in water, (III) the glittered LEDs powered by the TENG, and (IV) the pocket card light made by a TENG with a cantilever spring copper leaf. (b) V_{oc} of TENGs when the pressing is periodically changed at different frequencies. (c) Stable output of the TENG after long operation time.

TENG fabricated by APLF, a waterproof pocket card can be produced by this TENG with the cantilever spring leaf (Figure 4a-IV and Video S1). During pressing and releasing of the knob, the spring leaf under the knob deforms and recovers, which realizes contact and separation of the friction pairs, so the device is triggered. The self-powered card light based on the TENGs can offer lighting in emergency without an extra power source, thus providing convenience for emergency service.

Due to its high power, sensitivity, and stability, the TENG can also be used to monitor human sleep as a self-powered TES. For traditional sleep monitoring, the sensors usually require continuous use of electricity produced from an electric plug to achieve extreme sensitivities. Given that the TES can work without an extra power source, a monitoring device based on it can be designed and assembled smartly, offering great convenience for clinical diagnoses. Moreover, the whole cost can be greatly reduced due to the simple fabrication process and cheap raw materials of the TES. The TES can be fixed on a shoulder of a human body in order to detect the overturning movement during sleeping (Figure 5a and Video S2). The obvious drop of the generated V_{oc} output, which is caused by reducing the distance between two electrodes of the TES, indicates that the person turns over toward the side and the TES is pressed. During the person turning over in a supine posture, the pressure is released and the spring leaf rebounds, which results in the separation of the copper electrode from the APLF electrode. The movement would also be reflected in the change of V_{oc}. The leg movement can also be monitored by a TES fixed on a leg (Figure 5b and Video S3). Thus, by collecting the output voltage signal, the movement of the human can be simultaneously recorded and monitored. More importantly, ill people at home can be monitored remotely in real time by doctors in a hospital *via* Bluetooth, 4G, or WiFi, as illustrated in Figure S5. This sensitive system can achieve real-

DOI: 10.1021/acsnano.6b04344
ACS Nano XXXX, XXX, XXX−XXX

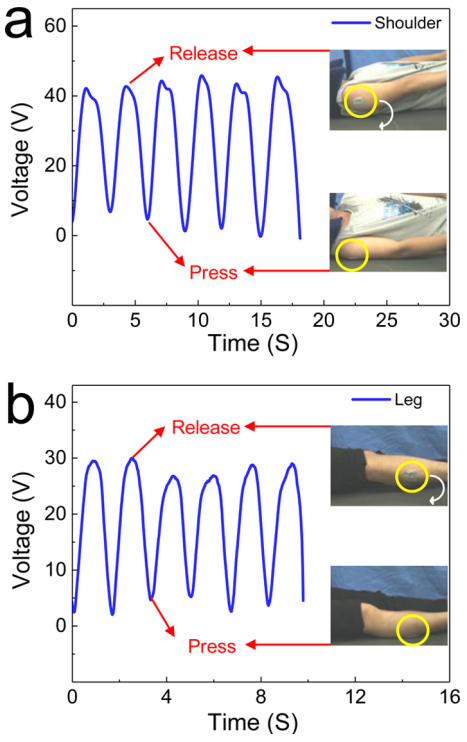

Figure 5. Application of the TES for sleep−body monitoring. Changes of voltage with time collected from the TES stuck onto different parts of a human body during sleep monitoring: (a) shoulder and (b) leg. Photographs of the TES stuck on a shoulder and a leg before and after overturning movement of the human body are shown in the insets.

time mobile healthcare services for the management of chronic disease, which will bring convenience and save time for the patients. This work only demonstrates the feasibility of the self-powered and sensitive sensors based on nanostructured TENGs for sleep−body monitoring during diagnosis of sleep disorders or body movement caused by sleep apnea. It can also be extended to real-time monitoring of other chronic diseases, such as monitoring hypertension, diabetes, encephalopathy and osteopathy, *etc.*

CONCLUSION

In summary, a high-performance structured TENG based on cheap APLF material with nanopillar arrays was fabricated by a scalable top-down thermoplastic forming process without extra deposition of a metal electrode. The sandwich structured TENG with an entrapped cantilever spring leaf rapidly responds to the extra pressure. The process of pressing from an external movement and release caused by self-recovering due to rebound leads to a triboelectric effect and charge separation between the APLF and the entrapped spring leaf. The open-circuit voltage generated from the structured APLF with nanopillars in a uniform diameter of 600 nm and a length of 1.5 μm has more than doubled to 55 V, so the sensitivity of the TENG is significantly improved. The sensitive and flexible TENG based on nanopillar arrays on APLF is easily packaged and used as a self-powered TES for monitoring overturning movement of a shoulder and a leg during sleeping. Due to the distinctive advantages of the TENG and delicate design of the sensor, this work may offer effective approaches to designing wearable electronic devices and improving their electric output performance and open the possibility for application in healthcare monitoring. These findings also provide a promising strategy to achieve real-time mobile healthcare services for the management of chronic diseases.

EXPERIMENTAL SECTION

Fabrication of the Nanopillar Arrays on the APLF Surface. Anodic aluminum oxide templates have uniform pore diameters of 400 and 700 nm and a depth of 5 μm. A piece of AAO template was placed on the top of the CPP surface of the APLF (Shenzhen KJ Group, China), where it was fixed tightly by a clamp and heated at 180 °C for 10 min in an oven. Subsequently, the templates were taken out and kept for at least 15 min at room temperature. The AAO template was softly removed from the APLF. Another surface of the APLF was polished carefully by an abrasive paper until the aluminum layer was exposed to connect a conducting wire. Finally, the obtained nanopillar arrays were rinsed with ethanol and dried in air.

Fabrication of Flexible TENGs. The APLF was folded, and the cantilever spring leaf was subsequently inserted. Both the top and bottom surfaces of the cantilever spring leaf, which has a middle plate with a diameter of 2 cm and a thickness of 50 μm, were fixed on the CPP layer. Finally, the other three sides of APLF were sealed by a heat-sealing machine (Shenzhen KJ Group, China).

Characterization and Measurement. The output voltage and current were measured by a Keithley system electrometer (Keithley 6514) and a Stanford low-noise current preamplifier (Model SR570), respectively.

ASSOCIATED CONTENT

Supporting Information

The Supporting Information is available free of charge on the ACS Publications website at DOI: 10.1021/acsnano.6b04344.

SEM images of AAO templates (Figure S1), nanopillar arrays (Figures S2, S3); photograph of the remote control and electric signals recorded by a cell phone (Figure S4); schematic illustration of self-powered triboelectric sensors for a wearable sleep monitoring system (Figure S5) (PDF)
Video S1 (MPG)
Video S2 (MPG)
Video S3 (MPG)

AUTHOR INFORMATION

Corresponding Authors

*E-mail: sunchunwen@binn.cas.cn.
*E-mail: zlwang@gatech.edu.

Notes

The authors declare no competing financial interest.

ACKNOWLEDGMENTS

This work was supported by the Thousands Talents Program for the pioneer researcher and his innovation team in China. The authors also acknowledge the financial support of the National Science Foundation of China (Nos. 51172275, 51372271, and 61404035), the National Key Basic Research Program of China (No. 2012CB215402), and the China Postdoctoral Science Foundation (2016M590070). We thank Prof. Helmuth Möhwald at Max-Planck-Institute of Colloids and Interfaces for helpful discussions.

REFERENCES

(1) Mahowald, M. W.; Schenck, C. H. Insights from Studying Human Sleep Disorders. *Nature* **2005**, *437*, 1279−1285.
(2) Viventi, J.; Kim, D. H.; Vigeland, L.; Frechette, E. S.; Blanco, J. A.; Kim, Y. S.; Avrin, A. E.; Tiruvadi, V. R.; Hwang, S. W.; Vanleer, A. C.;

DOI: 10.1021/acsnano.6b04344
ACS Nano XXXX, XXX, XXX−XXX

et al. Flexible, Foldable, Actively Multiplexed, High-Density Electrode Array for Mapping Brain Activity *in Vivo*. *Nat. Neurosci.* **2011**, *14*, 1599−1605.
(3) Dobrescu, A. I.; Ardelean, L.; Matei, C.; Tampa, M.; Puiu, M.; Mihaicusa, S. Polysomnography Test and Sleep Disordered Breathing in Prader-Willi Syndrome. *Materiale Plastice* **2014**, *51*, 331−335.
(4) Zi, Y. L.; Niu, S. M.; Wang, J.; Wen, Z.; Tang, W.; Wang, Z. L. Standards and Figure-of-Merits for Quantifying the Performance of Triboelectric Nanogenerators. *Nat. Commun.* **2015**, *6*, 8376.
(5) Zhu, G.; Peng, B.; Chen, J.; Jing, Q. S.; Wang, Z. L. Triboelectric Nanogenerators as a New Energy Technology: From Fundamentals, Devices, to Applications. *Nano Energy* **2015**, *14*, 126−138.
(6) Cai, F.; Yi, C. R.; Liu, S. C.; Wang, Y.; Liu, L. C.; Liu, X. Q.; Xu, X. M.; Wang, L. Ultrasensitive, Passive and Wearable Sensors for Monitoring Human Muscle Motion and Physiological Signals. *Biosens. Bioelectron.* **2016**, *77*, 907−913.
(7) Fan, F. R.; Tian, Z. Q.; Wang, Z. L. Flexible Triboelectric Generator! *Nano Energy* **2012**, *1*, 328−334.
(8) Taghavi, M.; Sadeghi, A.; Mondini, A.; Mazzolai, B.; Beccai, L.; Mattoli, V. Triboelectric Smart Machine Elements and Self-Powered Encoder. *Nano Energy* **2015**, *13*, 92−102.
(9) Zhu, H. R.; Tang, W.; Gao, C. Z.; Han, Y.; Li, T.; Cao, X.; Wang, Z. L. Self-Powered Metal Surface Anti-Corrosion Protection Using Energy Harvested from Rain Drops and Wind. *Nano Energy* **2015**, *14*, 193−200.
(10) Zhong, X. D.; Yang, Y.; Wang, X.; Wang, Z. L. Rotating-Disk-Based Hybridized Electromagnetic-Triboelectric Nanogenerator for Scavenging Biomechanical Energy as a Mobile Power Source. *Nano Energy* **2015**, *13*, 771−780.
(11) Zheng, L.; Cheng, G.; Chen, J.; Lin, L.; Wang, J.; Liu, Y. S.; Li, H. X.; Wang, Z. L. A Hybridized Power Panel to Simultaneously Generate Electricity from Sunlight, Raindrops, and Wind around the Clock. *Adv. Energy Mater.* **2015**, *5*, 1501152.
(12) Mao, Y. C.; Geng, D. L.; Liang, E. J.; Wang, X. D. Single-Electrode Triboelectric Nanogenerator for Scavenging Friction Energy from Rolling Tires. *Nano Energy* **2015**, *15*, 227−234.
(13) Seol, M. L.; Woo, J. H.; Jeon, S. B.; Kim, D.; Park, S. J.; Hur, J.; Choi, Y. K. Vertically Stacked Thin Triboelectric Nanogenerator for Wind Energy Harvesting. *Nano Energy* **2015**, *14*, 201−208.
(14) Liang, Q. J.; Yan, X. Q.; Gu, Y. S.; Zhang, K.; Liang, M. Y.; Lu, S. N.; Zheng, X.; Zhang, Y. Highly Transparent Triboelectric Nanogenerator for Harvesting Water-Related Energy Reinforced by Antireflection Coating. *Sci. Rep.* **2015**, *5*, 9080.
(15) Liang, Q.; Yan, X.; Liao, X.; Zhang, Y. Integrated Multi-Unit Transparent Triboelectric Nanogenerator Harvesting Rain Power for Driving Electronics. *Nano Energy* **2016**, *25*, 18−25.
(16) López-Suárez, M.; Abadal, G.; Gammaitoni, L.; Rurali, R. Noise Energy Harvesting in Buckled BN Nanoribbons from Molecular Dynamics. *Nano Energy* **2015**, *15*, 329−334.
(17) Zhong, Q. Z.; Zhong, J. W.; Hu, B.; Hu, Q. Y.; Zhou, J.; Wang, Z. L. A Paper-Based Nanogenerator as a Power Source and Active Sensor. *Energy Environ. Sci.* **2013**, *6*, 1779−1784.
(18) Yu, A. F.; Chen, X. Y.; Wang, R.; Liu, J. Y.; Luo, J. J.; Chen, L. B.; Zhang, Y.; Wu, W.; Liu, C. H.; Yuan, H. T.; et al. Triboelectric Nanogenerator as a Self-Powered Communication Unit for Processing and Transmitting Information. *ACS Nano* **2016**, *10*, 3944−3950.
(19) Pang, Y. K.; Li, X. H.; Chen, M. X.; Han, C. B.; Zhang, C.; Wang, Z. L. Triboelectric Nanogenerators as a Self-Powered 3d Acceleration Sensor. *ACS Appl. Mater. Interfaces* **2015**, *7*, 19076−19082.
(20) Lee, K. Y.; Yoon, H.-J.; Jiang, T.; Wen, X.; Seung, W.; Kim, S.-W.; Wang, Z. L. Fully Packaged Self-Powered Triboelectric Pressure Sensor Using Hemispheres-Array. *Adv. Energy Mater.* **2016**, *6*, 1502566.
(21) Wang, Z. L. Triboelectric Nanogenerators as New Energy Technology for Self-Powered Systems and as Active Mechanical and Chemical Sensors. *ACS Nano* **2013**, *7*, 9533−9557.
(22) Yang, P. K.; Lin, L.; Yi, F.; Li, X. H.; Pradel, K. C.; Zi, Y. L.; Wu, C. I.; He, J. H.; Zhang, Y.; Wang, Z. L. A Flexible, Stretchable and Shape-Adaptive Approach for Versatile Energy Conversion and Self-Powered Biomedical Monitoring. *Adv. Mater.* **2015**, *27*, 3817−3824.
(23) Guo, W. X.; Li, X. Y.; Chen, M. X.; Xu, L.; Dong, L.; Cao, X.; Tang, W.; Zhu, J.; Lin, C. J.; Pan, C. F.; et al. Electrochemical Cathodic Protection Powered by Triboelectric Nanogenerator. *Adv. Funct. Mater.* **2014**, *24*, 6691−6699.
(24) Yi, F.; Lin, L.; Niu, S. M.; Yang, J.; Wu, W. Z.; Wang, S. H.; Liao, Q. L.; Zhang, Y.; Wang, Z. L. Self-Powered Trajectory, Velocity, and Acceleration Tracking of a Moving Object/Body Using a Triboelectric Sensor. *Adv. Funct. Mater.* **2014**, *24*, 7488−7494.
(25) Kim, K. N.; Chun, J.; Kim, J. W.; Lee, K. Y.; Park, J. U.; Kim, S. W.; Wang, Z. L.; Baik, J. M. Highly Stretchable 2D Fabrics for Wearable Triboelectric Nanogenerator under Harsh Environments. *ACS Nano* **2015**, *9*, 6394−6400.
(26) Meng, B.; Tang, W.; Too, Z. H.; Zhang, X. S.; Han, M. D.; Liu, W.; Zhang, H. X. A Transparent Single-Friction-Surface Triboelectric Generator and Self-Powered Touch Sensor. *Energy Environ. Sci.* **2013**, *6*, 3235−3240.
(27) Li, S. L.; Zhong, Q. Z.; Zhong, J. W.; Cheng, X. F.; Wang, B.; Hu, B.; Zhou, J. Cloth-Based Power Shirt for Wearable Energy Harvesting and Clothes Ornamentation. *ACS Appl. Mater. Interfaces* **2015**, *7*, 14912−14916.
(28) Lin, L.; Xie, Y. N.; Niu, S. M.; Wang, S. H.; Yang, P. K.; Wang, Z. L. Robust Triboelectric Nanogenerator Based on Rolling Electrification and Electrostatic Induction at an Instantaneous Energy Conversion Efficiency of Similar to 55%. *ACS Nano* **2015**, *9*, 922−930.
(29) Ko, Y. H.; Nagaraju, G.; Lee, S. H.; Yu, J. S. PDMS-Based Triboelectric and Transparent Nanogenerators with ZnO Nanorod Arrays. *ACS Appl. Mater. Interfaces* **2014**, *6*, 6631−6637.
(30) Zhang, C.; Li, J.; Han, C. B.; Zhang, L. M.; Chen, X. Y.; Wang, L. D.; Dong, G. F.; Wang, Z. L. Organic Tribotronic Transistor for Contact-Electrification-Gated Light-Emitting Diode. *Adv. Funct. Mater.* **2015**, *25*, 5625−5632.
(31) Wei, X. Y.; Zhu, G.; Wang, Z. L. Surface-Charge Engineering for High-Performance Triboelectric Nanogenerator Based on Identical Electrification Materials. *Nano Energy* **2014**, *10*, 83−89.
(32) Lee, S.; Hinchet, R.; Lee, Y.; Yang, Y.; Lin, Z.-H.; Ardila, G.; Montès, L.; Mouis, M.; Wang, Z. L. Ultrathin Nanogenerators as Self-Powered/Active Skin Sensors for Tracking Eye Ball Motion. *Adv. Funct. Mater.* **2014**, *24*, 1163−1168.
(33) Zhang, A. H.; Liu, W.; Zhang, Y. On the Mechanism and Optimization of Triboelectric Nanogenerators. *Nanotechnology* **2015**, *26*, 425401.
(34) Liu, Y.; Niu, S. M.; Wang, Z. L. Theory of Tribotronics. *Adv. Electron. Mater.* **2015**, *1*, 1500124.
(35) Lee, K. Y.; Gupta, M. K.; Kim, S. W. Transparent Flexible Stretchable Piezoelectric and Triboelectric Nanogenerators for Powering Portable Electronics. *Nano Energy* **2015**, *14*, 139−160.
(36) Su, Y. J.; Yang, Y.; Zhang, H. L.; Xie, Y. N.; Wu, Z. M.; Jiang, Y. D.; Fukata, N.; Bando, Y.; Wang, Z. L. Enhanced Photodegradation of Methyl Orange with TiO_2 Nanoparticles Using a Triboelectric Nanogenerator. *Nanotechnology* **2013**, *24*, 295401.
(37) Li, W.; Chen, T.; Xu, W. On Impedance Matching and Maximum Power Transfer. *Electr. Power Syst. Res.* **2010**, *80*, 1082−1088.
(38) Kim, Y. G.; Nam, S. Spherical Mode-Based Analysis of Wireless Power Transfer between Two Antennas. *IEEE Trans. Antennas Propag.* **2014**, *62*, 3054−3063.
(39) Mannsfeld, S. C. B.; Tee, B. C. K.; Stoltenberg, R. M.; Chen, C. V. H. H.; Barman, S.; Muir, B. V. O.; Sokolov, A. N.; Reese, C.; Bao, Z. Highly Sensitive Flexible Pressure Sensors with Microstructured Rubber Dielectric Layers. *Nat. Mater.* **2010**, *9*, 859−864.
(40) Fan, F. R.; Lin, L.; Zhu, G.; Wu, W. Z.; Zhang, R.; Wang, Z. L. Transparent Triboelectric Nanogenerators and Self-Powered Pressure Sensors Based on Micropatterned Plastic Films. *Nano Lett.* **2012**, *12*, 3109−3114.
(41) Barbuzzi, G.; Grimaldi, F.; Del Nobile, M. A. Quality Decay of Fresh Processed Fish Stored under Refrigerated Conditions. *J. Food Saf.* **2009**, *29*, 271−286.

DOI: 10.1021/acsnano.6b04344
ACS Nano XXXX, XXX, XXX−XXX